A comparison of ocean emissivity models using the Advanced Microwave Sounding Unit, the Special Sensor Microwave Imager, the TRMM Microwave Imager, and airborne radiometer observations

W. J. Ellison,[1] S. J. English,[2] K. Lamkaouchi,[3] A. Balana,[4] E. Obligis,[5] G. Deblonde,[6] T. J. Hewison,[2] P. Bauer,[7] G. Kelly,[7] and L. Eymard[8]

Received 25 November 2002; revised 4 March 2003; accepted 8 April 2003; published 5 November 2003.

[1] New measurements of the permittivity of saline water at millimeter wavelengths have the potential to improve the accuracy of ocean surface emissivity models for use with microwave and millimeter-wave imaging and sounding instruments. Recent radiative transfer models employing a range of different treatments of surface ocean emissivity are compared with observations from the following microwave radiometers: Advanced Microwave Sounding Unit, Special Sensor Microwave Imager, TRMM Microwave Imager, Microwave Airborne Radiometer Scanning System, and Deimos. Emissivity models using the new permittivity model fit these observations more closely than those models which use the Klein and Swift extrapolation model. *INDEX TERMS:* 3337 Meteorology and Atmospheric Dynamics: Numerical modeling and data assimilation; 3339 Meteorology and Atmospheric Dynamics: Ocean/atmosphere interactions (0312, 4504); 3359 Meteorology and Atmospheric Dynamics: Radiative processes; 3360 Meteorology and Atmospheric Dynamics: Remote sensing; 3394 Meteorology and Atmospheric Dynamics: Instruments and techniques; *KEYWORDS:* permittivity, microwave, AMSU, SSM/I, TMI, MARSS

Citation: Ellison, W. J., S. J. English, K. Lamkaouchi, A. Balana, E. Obligis, G. Deblonde, T. J. Hewison, P. Bauer, G. Kelly, and L. Eymard, A comparison of ocean emissivity models using the Advanced Microwave Sounding Unit, the Special Sensor Microwave Imager, the TRMM Microwave Imager, and airborne radiometer observations, *J. Geophys. Res.*, *108*(D21), 4663, doi:10.1029/2002JD003213, 2003.

1. Introduction

[2] Passive microwave radiometers such as the Advanced Microwave Sounding Unit (AMSU) and Special Sensor Microwave Imager (SSM/I) provide information on temperature, humidity, and surface wind speed over data sparse ocean regions. This information has been used to improve the accuracy of Numerical Weather Prediction (NWP) models [*English et al.*, 2000]. Information on temperature in the lowest 3 km of the atmosphere rises by a factor of 2 as the surface emissivity errors fall from 0.020 to 0.005 [*English*, 1999]. The accuracy of the ocean surface emissivity model depends upon many factors. This paper will focus upon one of them: the permittivity of saline water. Existing models [*Klein and Swift*, 1977; *Liebe et al.*, 1991; *Stogryn et al.*, 1995] used for frequencies between 10 and 200 GHz are extrapolation functions based upon laboratory measurements below 10 GHz. In section 2, permittivity measurements of seawater at frequencies up to 105 GHz made at the Laboratoire de Physique des Interactions Ondes-Matière (PIOM) will be described. These measurements have been incorporated into a fast ocean emissivity model [*English and Hewison*, 1998; *Deblonde and English*, 2000] which is used at several operational NWP centers to assist in the simulation of microwave brightness temperature measurements. In section 3 measurements from the Advanced Microwave Sounding Unit (AMSU), the Special Sensor Microwave Imager (SSM/I), the TRMM Microwave Imager (TMI) and airborne radiometers, MARSS [*McGrath and Hewison*, 2001] and Deimos [*Hewison*, 1995] are compared with simulations using different emissivity models. Some of the comparisons are clean tests of different permittivity models and some comparisons also change other components of the emissivity model. At wind speeds below 7 m s^{-1} the choice of permittivity model has the largest impact upon the microwave brightness temperature. In section 4 the

[1]Physique des Interactions Ondes Matières, Ecole Nationale Supérieure de Chimie et de Physique de Bordeaux, Pessac, France.
[2]Met Office, Exeter, UK.
[3]Faculty of Sciences, University of Meknès, Morocco.
[4]Centre d'études nucléaires de Bordeaux Gradignan, Gradignan, France.
[5]Space Oceanography Division, Collecte Localisation Satellites, Ramonville St-Agne, France.
[6]Meteorological Service of Canada, Dorval, Quebec, Canada.
[7]European Centre for Medium-Range Weather Forecasts, Reading, UK.
[8]Centre d'étude des Environnements Terrestre et Planétaires/Institut Pierre Simon Laplace/Centre National de la Recherche Scientifique, Université St Quentin-Versailles, Vélizy, France.

0148-0227/03/2002JD003213$09.00

Table 1. Permittivity Data for Seawater Over the Frequency Range 30–105 GHz and Over the Temperature Range −2°, 5°, 10°, and 15°C

	−2°C		5°C		10°C		15°C	
GHz	ε'	ε''	ε'	ε''	ε'	ε''	ε'	ε''
30.0	13.92	21.60	16.10	25.00	19.31	28.43	20.88	29.25
33.0	12.24	20.60	14.95	23.84	16.84	26.86	19.14	28.51
35.0	11.92	20.41	14.47	22.73	16.36	26.31	18.80	27.24
37.0	10.66	19.46	14.32	22.00	15.73	24.48	17.64	26.04
40.0	10.20	18.26	13.37	20.81	13.94	22.80	16.65	24.10
45.0	9.79	16.00	12.21	18.85	12.80	21.11	14.20	22.95
48.0	9.56	15.32	11.21	18.03	12.20	19.81	12.90	21.80
50.0	9.27	14.50	10.72	17.50	11.60	18.62	11.36	20.76
52.0	8.91	13.72	10.60	16.80	10.81	17.55	10.77	19.87
55.0	8.80	12.70	10.43	16.30	10.51	17.00	10.60	18.93
57.3	8.73	12.63	10.00	15.93	10.33	16.50	10.33	18.60
60.0	8.60	12.35	9.88	15.52	10.10	16.15	10.00	18.54
64.0	8.40	11.90	9.48	14.40	9.70	15.96	9.83	17.65
65.0	8.28	11.70	9.35	14.31	9.53	15.75	9.70	17.40
66.0	8.11	11.55	9.10	13.80	9.24	15.24	9.45	17.27
70.0	8.05	11.22	8.53	13.50	9.00	14.73	9.50	16.05
73.0	7.88	11.15	8.30	12.90	8.76	14.44	9.75	15.89
75.0	7.75	10.70	8.10	12.66	8.54	14.10	8.80	15.50
78.0	7.60	10.48	7.90	12.32	8.38	13.60	9.20	14.80
80.0	7.45	10.05	7.84	11.97	8.20	13.20	9.00	14.55
82.0	7.36	9.83	7.75	11.83	8.10	12.86	8.55	13.60
85.5	7.30	9.60	7.64	11.12	7.90	12.54	8.27	13.45
87.0	7.16	9.55	7.51	10.82	7.73	12.20	8.30	13.44
89.0	7.43	9.38	7.24	10.62	7.64	11.84	8.12	13.36
92.0	7.28	9.00	7.17	10.54	7.48	11.72	7.90	13.00
94.0	7.18	8.84	7.13	10.35	7.35	11.22	7.60	12.94
95.0	6.82	8.60	6.83	10.15	7.40	11.11	7.50	12.44
97.0	7.15	8.55	7.07	9.90	7.52	10.92	7.65	12.31
100.0	7.05	8.26	7.05	9.60	7.25	10.54	7.30	11.88
103.0	6.93	8.11	7.06	9.48	7.31	10.36	7.41	11.56
105.0	6.73	8.01	7.00	9.38	7.20	10.16	7.56	11.18

results of the comparisons are summarized and the main conclusions presented.

2. New Permittivity Measurements

[3] In the work of *Ellison et al.* [1996, 1998] an interpolation model for the permittivity of natural seawater, valid in the frequency range $3 \leq \nu \leq 37$ GHz, the temperature range $-2 \leq T \leq 30$°C, and the salinity range 20‰ $\leq S \leq$ 40‰ was described. It was felt that this model could not be extrapolated to higher frequencies with an acceptable accuracy and that further experimental data would be necessary. The effect of salinity variations in the range 20–40‰ upon the measured permittivity decreases as the frequency increases. From ~30 GHz a variation in the salinity in this range produces a variation in the measured permittivity which is much smaller than the 3% experimental uncertainty. For this reason, between 30 and 105 GHz the permittivity was measured at a unique salinity, namely its mean value, 35‰. It was also shown that the difference in permittivity between natural seawater and synthetic seawater made according to the recipe given by *Grassholf* [1976] was less than the 1% experimental error over the frequency range 3–20 GHz and a fortiori less than the 3% experimental error for higher frequencies.

2.1. The New Permittivity Measurements in the Frequency Range 30–105 GHz

[4] The ABmm measuring system, described by *Ellison et al.* [1997] and *Lamkaouchi et al.* [2003], was used to determine the permittivity of synthetic seawater with a salinity of 35/1000 in ~2 GHz steps from 30 to 105 GHz and at temperatures of −2°, 5°, 10°, 15°, 20°, 25°, and 30°C. It is shown by *Lamkaouchi et al.* [2003] that this system is capable of producing permittivity data for aqueous solutions with a dispersion of ~3% about the true value. The numerical data is given in Tables 1 and 2.

[5] The lack of permittivity data for frequencies greater than ~20 GHz obliged one to extrapolate permittivity models valid only at relatively low frequencies. As we shall see below, this extrapolation leads to substantal errors in the permittivity values.

[6] In order to compare the measured values in the frequency range 30–105 GHz with extrapolated values of a permittivity model valid in the frequency range 3–20 GHz, we also measured the permittivity of synthetic seawater over this frequency range and over the temperature range −2 to 30°C in 1°C steps. This was done using the Hewlett-Packard measuring system described by *Ellison et al.* [1997] and *Lamkaouchi et al.* [2003]. The appropriate permittivity model is that of Debye:

$$\varepsilon(\nu,t) = \varepsilon'(\nu,t) - j\varepsilon''(\nu,t) = \frac{\varepsilon_s - \varepsilon_\infty}{1 + j.2\pi\tau\nu} - j\left(\frac{\sigma}{2\pi\varepsilon^*\nu}\right) + \varepsilon_\infty.$$

The corresponding parameters for each temperature are given in Table 3. In Figure 1 we show the comparison

Table 2. Permittivity Data for Seawater Over the Frequency Range 30–105 GHz and Over the Temperature Range 20°, 25°, and 30°C

	20°C		25°C		30°C	
GHz	ε'	ε''	ε'	ε''	ε'	ε''
30.0	24.32	30.60	26.83	31.97	30.07	33.55
33.0	21.52	29.82	24.56	31.31	27.70	32.02
35.0	20.60	29.16	22.73	30.26	24.40	31.84
37.0	19.32	28.44	19.40	28.21	21.71	30.24
40.0	17.45	27.30	18.20	27.50	20.11	29.27
45.0	14.97	25.18	16.26	25.20	18.40	28.57
48.0	13.57	23.78	15.37	24.62	17.45	27.22
50.0	12.90	23.32	14.80	23.77	16.48	26.94
52.0	12.54	22.26	14.36	22.40	15.80	26.72
55.0	12.23	21.62	13.95	21.92	15.58	25.32
57.3	12.06	20.60	13.78	21.72	14.74	24.60
60.0	11.84	20.08	13.57	21.47	14.21	22.88
64.0	11.60	19.55	12.82	20.63	13.35	21.97
65.0	11.45	19.23	12.60	20.37	12.90	21.60
66.0	11.36	18.74	12.80	19.42	12.70	20.85
70.0	10.78	17.53	12.31	18.76	12.10	20.64
73.0	10.16	17.10	11.00	18.50	11.33	19.96
75.0	10.47	16.50	10.68	17.56	11.13	18.80
78.0	9.95	16.20	10.21	17.00	10.76	18.40
80.0	9.76	15.56	10.11	16.78	10.30	18.67
82.0	9.40	14.85	10.00	16.13	10.28	17.78
85.5	9.30	14.77	9.66	15.75	10.22	17.45
87.0	8.90	14.46	9.50	15.45	9.70	17.10
89.0	8.77	14.26	9.34	15.27	9.51	16.56
92.0	8.52	14.05	9.05	15.10	9.37	16.07
94.0	8.12	13.23	8.90	14.75	9.12	15.77
95.0	8.00	13.68	8.80	14.70	9.00	15.70
97.0	7.95	13.40	8.40	14.44	8.91	14.93
100.0	7.86	12.85	8.34	13.80	8.62	15.12
103.0	7.73	13.00	8.25	13.48	8.48	14.61
105.0	7.67	12.60	8.12	13.70	8.74	14.88

Table 3. Parameters for the Debye Model in the Range 3–20 GHz

deg. Celsius	τ, psecs	ε_∞	ε_s
−2.04	18.58	8.264	79.548
−1.00	17.96	8.639	79.762
0.03	17.14	8.271	78.914
0.97	16.40	7.837	78.038
2.00	15.81	7.814	77.710
2.98	15.27	7.830	77.432
4.01	14.74	7.827	77.132
5.03	14.22	7.788	76.806
6.00	13.73	7.674	76.404
7.00	13.28	7.644	76.099
7.99	12.88	7.671	75.868
9.02	12.46	7.633	75.555
10.02	12.06	7.550	75.207
11.03	11.68	7.492	74.878
12.02	11.34	7.433	74.561
13.02	11.00	7.368	74.229
14.02	10.69	7.385	73.993
15.01	10.42	7.464	73.790
17.00	9.908	7.606	73.365
18.03	9.655	7.656	73.126
19.01	9.431	7.761	72.921
20.02	9.216	7.912	72.731
21.02	9.026	8.084	72.529
22.00	8.857	8.332	72.366
22.99	8.690	8.541	72.171
23.96	8.541	8.812	72.021
25.02	8.394	9.129	71.845
26.00	8.280	9.531	71.716
27.01	8.188	10.069	71.654
28.02	8.102	10.546	71.502
29.03	7.990	10.876	71.331
29.98	7.855	10.900	70.909

between the measured data and the corresponding Debye model. In Figure 2 we compare the measured permittivity data in the frequency range 30–105 GHz at −2°C with the extrapolated Debye model. Clearly the extrapolated values differ from the measured data. This is true at all temperatures. The differences do, however, decrease as the temperature increases from −2° to 30°C. We conclude that the simple Debye model valid for "low" frequencies cannot be adequately extrapolated so as to represent the data over the complete frequency range.

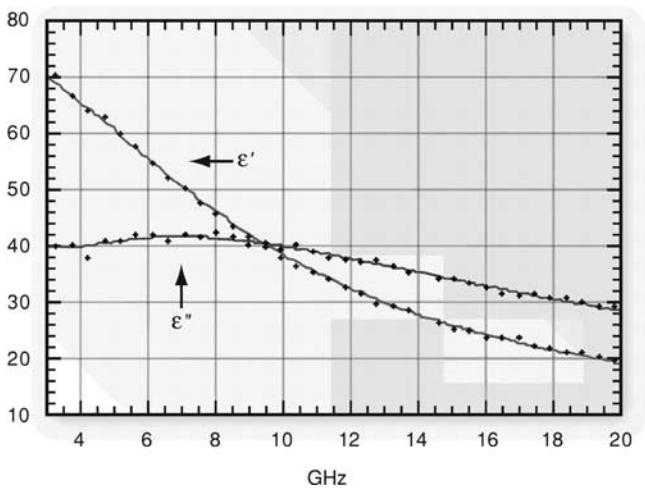

Figure 1. Fit of the single Debye model to new permittivity measurements below 20 GHz. See color version of this figure in the HTML.

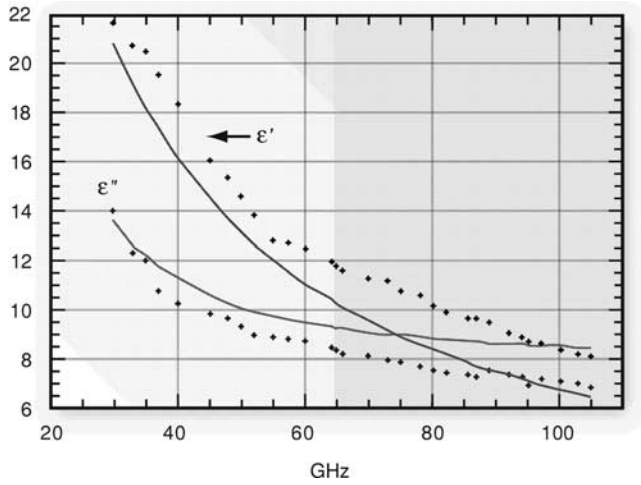

Figure 2. Extrapolation of the single Debye model to permittivity measurements above 30 GHz. See color version of this figure in the HTML.

[7] The question is, what type of function does represent the data? There are some theoretical reasons [*Haggis et al.*, 1952; *Grant and Sheppard*, 1974; *Barthel et al.*, 1990] to suspect that there may be a second Debye relaxation for pure water "somewhere in the far or very far infrared." However, there is practically no experimental data to either confirm or refute the "second Debye" hypothesis. The only reliable data is that of *Barthel et al.* [1991, 1992], at 25°C, who interpret their data with a second Debye term with a relaxation time of 1 psec (∼160 GHz for the relaxation frequency). Thus it is reasonable to try and fit our experimental data for synthetic seawater with a salinity of 35/1000 in the frequency range 3–105 GHz with a double Debye model.

[8] At each of the seven temperatures we fitted the experimental data to the model

$$\varepsilon(\nu,t) = \varepsilon'(\nu,t) - j\varepsilon''(\nu,t) = \frac{\Delta_1}{1+j(2\pi\tau_1\nu)} + \frac{\Delta_2}{1+j(2\pi\tau_2\nu)} - j\left(\frac{\sigma}{2\pi\varepsilon^*\nu}\right) + \varepsilon_\infty,$$

where the frequency ν is in hertz, the relaxation times are in seconds, $\varepsilon^* = 8.854 \times 10^{-12}$, and σ, the conductivity of the synthetic seawater in Siemens per meter, as a function of the temperature T, is given by $\sigma = 2.906 + 0.09437T$. The best "least squares" fitting for the parameters is given in Table 4.

Table 4. Parameters for the Double Debye Model

deg. Celsius	$\tau_1 \times 10^{12}$	$\tau_2 \times 10^{12}$	Δ_1	Δ_2	ε_s	ε_∞
−2	18.85	3.104	69.361	4.298	79.008	5.348
5	14.71	2.943	66.748	4.826	76.797	5.223
10	12.15	2.807	66.104	3.698	74.956	5.154
15	10.14	1.637	65.752	2.368	73.048	4.929
20	8.877	1.327	65.194	1.163	71.609	5.253
25	7.845	0.974	64.046	0.669	70.293	5.578
30	6.936	0.911	62.503	1.848	68.871	4.520

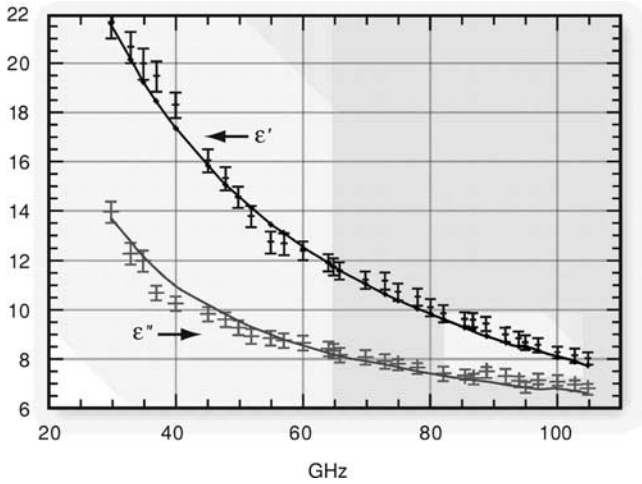

Figure 3. Comparison of the double Debye model and the new measurements above 30 GHz at T = −2°C. See color version of this figure in the HTML.

[9] The temperature dependence of each parameter was found by regression against temperature polynomials

$$\tau_1 \times 10^{12} = 17.535 - 0.61767T + 0.0089481T^2,$$

$$\tau_2 \times 10^{12} = 3.1842 + 0.019189T - 0.010873T^2 + 0.00025818T^3,$$

$$\Delta_1 = 68.396 - 0.40643T + 0.022832T^2 - 0.00053061T^3,$$

$$\Delta_2 = 4.7629 + 0.1541T - 0.033717T^2 + 0.00084428T^3.$$

Figures 3 and 4 compare the measured data and the double Debye interpolation at −2° and 5°C. The "goodness of fit" is similar at all the other temperatures.

[10] The above interpolation model was established for synthetic seawater with a salinity of 35/1000 and is valid for the frequency range 3–105 GHz and the temperature range −2° to 30°C. For frequencies in the range 30–105 GHz the permittivity values (for the 3% precision of the data) can be considered to be independent of the salinity, so the formula can be used for any salinity in this frequency range. For the frequency range 3–20 GHz the influence of the second Debye term is negligible, but the effect of salinity variations cannot be ignored. One should use the interpolation function for $\varepsilon(\nu, T, S)$ given by *Ellison et al.* [1998]. (We take this opportunity to correct a typographical error in the published formula: The exprression on page 643 of *Ellison et al.* [1998], $\varepsilon_0(t, S) = a_1(t) + S.a_2(t)$, should read $\varepsilon_0(t, S) = a_1(t) - S.\ a_2(t)$).

2.2. Extrapolation of the Model to the Frequency Range 100–500 GHz

[11] The double Debye function gives a good interpolation for the permittivity of seawater in the frequency range 30–100 GHz, and it is natural to inquire whether the extrapolated values of this function to higher frequencies corresponds to realistic permittivity values. The second Debye relaxation which we have detected with our measurements up to 100 GHz has its maximum effect at a peak somewhere between 100 and 200 GHz, depending upon the temperature. Error in the measurements gives a large error in the position of the frequency peak. Errors in the peak frequency are then transformed into errors in the value of ε''. Thus the extrapolated values will give better estimates of ε' than ε'' but the level of accuracy cannot be reliably estimated. There is no permittivity data for seawater at frequencies >100 GHz with which to characterize the error. The difference between seawater and pure water at these frequencies is probably small, and one can gain some insight about the validity of the extrapolations by comparing them to the permittivity values of pure water.

3. Comparison of Emissivity Models Against Microwave Radiometer Measurements

3.1. Description of Models Used in This Paper

[12] This paper brings together a number of results from different centers, all using slightly different implementations of the radiative transfer model. The calculations from the models are compared to observations from satellite radiometers (AMSU, SSM/I, and TMI) and aircraft radiometers (MARSS and Deimos). This section briefly describes each configuration used, listed in Table 5. Note that different models for atmospheric absorption can be used, and these are referred to in the relevant sections.

[13] RTSSMI_KS is the model developed at the European Centre for Medium-Range Weather Forecasts (ECMWF) for assimilation of measurements made by the SSM/I [*Phalippou*, 1993]. RTTOV [*Eyre*, 1991; *Saunders et al.*, 2002] is a model used for operational processing of Advanced TIROS Operational Vertical Sounder (ATOVS) and other instruments at several NWP centers [e.g., *English et al.*, 2000] and includes an ocean emissivity model [*English and Hewison*, 1998; *Deblonde and English*, 2000]. In section 3.6 a line-by-line model known as Radiative Transfer Microwave Model (RTM) was used. RTM uses *Liebe* [1989] for water absorption and *Liebe et al.* [1992] for

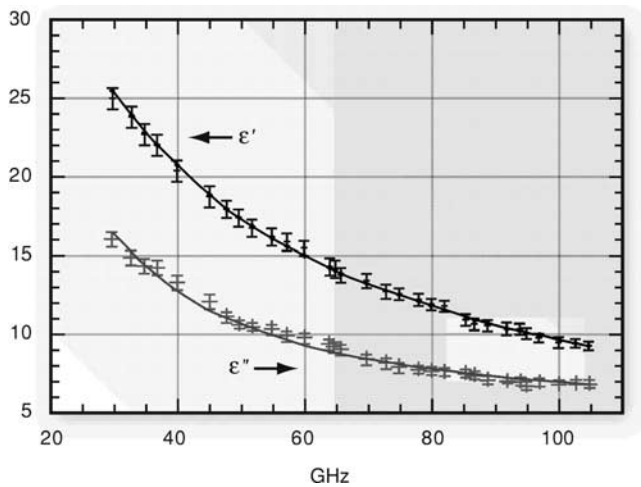

Figure 4. Comparison of the double Debye model and the new measurements above 30 GHz at T = 5°C. See color version of this figure in the HTML.

Table 5. Models Used in Section 3[a]

Name Used to Refer to Each Model Configuration in This Paper	Emissivity Model	Permittivity Model	Foam Model	Treatment of Geometric Roughness	Multiple Reflections	Section and Observations Tested
RTTOV_NEW	§1	see section 2	§2	Linear regression versus GO model	$(1 - R_p^2)$, $Tb^{\downarrow}$ ($\theta = 0$)	3.4 versus AMSU, 3.5 versus SSM/I, 3.6 versus MARSS, 3.6 versus Deimos
RTTOV_ULABY	§3	§4	§5		not applicable	3.4 versus AMSU
RTSSMI_KS	§5	§4	§6	GO model	$Tb^{\downarrow}$ = SSt	3.5 versus SSM/I, 3.6 versus MARSS, 3.6 versus Deimos
GUILLOU_ELLISON	§7	§8	§2	GO model	$(1 - R_p^2)$, $Tb^{\downarrow}$ ($\theta = 0$)	3.3 versus TMI
GUILLOU_NEW	§7	see section 2	§2	GO model	$(1 - R_p^2)$, $Tb^{\downarrow}$ ($\theta = 0$)	3.3 versus TMI

[a]GO, Geometric Optics; *T*skin, skin temperature; R_p, polarized reflectivity; $Tb^{\downarrow}$, downwelling brightness temperature; §1, *Deblonde and English* [2000]; §2, *Saunders et al.* [2002]; §3, *Weng et al.* [2000]; §4, *Klein and Swift* [1977]; §5, *Phalippou* [1996]; §6, *Karstens et al.* [1994]; §7, *Guillou et al.* [1998]; §8, *Ellison et al.* [1998]; AMSU, Advanced Microwave Sounding Unit; SSM/I, Special Sensor Microwave Imager; TMI, TRMM Microwave Imager.

oxygen, as does RTTOV. RTM uses a line-by-line atmospheric absorption model, and a geometric optics emissivity model, whereas RTTOV uses fast regression based fit to the output of such models. Differences between RTTOV and RTM are negligible and for simplicity we shall not make any further distinction between RTM and RTTOV in discussion, although it will be made clear if results are from an RTTOV or an RTM run. RTTOV and RTM can be run with different permittivity models and the naming convention is given in Table 5. Note that RTTOV_NEW is the distributed and supported version of RTTOV [*Saunders et al.*, 2002]. A detailed comparison of RTSSMI_KS and RTTOV_NEW is available from *Deblonde* [2000] where it was found that brightness temperature differences between the RTSSMI and RTTOV setup are largely dominated by the choice of the permittivity for surface wind speeds ≤ 7 m s^{-1}. The Bragg scattering impacts mostly the low frequencies and becomes important for wind speeds >7 m s^{-1}. The addition of the Bragg scattering effect leads to higher surface brightness temperatures. The formulation of foam cover is quite different in the RTSSMI and RTTOV/RTM setups. The foam cover for RTSSMI is much larger for high wind speeds than that of RTTOV/RTM. Higher amounts of foam cover imply a higher emissivity and consequently for channels that see the surface this will lead to higher emissivities; thus brightness temperatures will be higher for RTSSMI at high wind speeds (>7m s^{-1}). The RTSSMI multiple reflection parameterization will always lead to higher brightness temperatures than those of RTTOV. The percentage of facets for which multiple reflection occurs increases rapidly with incidence angle. GUILLOU_NEW is very similar to the RTTOV_NEW and GUILLOU_ELLISON is similar to RTTOV_ELLISON.

3.2. Description of Observations Used in This Study

[14] In sections 3.3–3.6, observations are used from several microwave radiometer systems. The Advanced Microwave Sounding Unit (AMSU) is a 20 channel microwave radiometer operating from National Oceanic and Atmospheric Administration (NOAA) polar orbiting satellites since 1998. It has a cross-track scan mechanism, so the emissivity has to be modeled at a range of incidence angles. A single polarization is measured which is a mixture of vertical and horizontal polarization determined by the instrument nadir angle. It has surface-sensing channels at 23.8, 31.4, 50.3, 52.4, 89, and 150 GHz. The Special Sensor Microwave Imager (SSM/I) is a conically scanning microwave radiometer which is dual polarized with a fixed incidence angle. It operates on the Defense Meteorological Satellite Program (DMSP) polar orbiting satellites. It has channels at 19.35, 22.235, 37, and 85.5 GHz. The 22.235 GHz channel only measures vertical polarization. The TRMM Microwave Imager is similar to SSM/I but has a lower inclination, so it only provides observations in the tropics and part of the extratropics, up to 40°N/S. It also has a channel at 10.7 GHz. MARSS is a two-channel airborne radiometer at 89 and 150 GHz with an along-track scan mechanism and single polarization. For the observations used here it operated on the C-130 aircraft of the Met research flight. Deimos is a two-channel dual-polarized radiometer at 23.8 and 50.1 GHz, also operated on the C-130 of the Met research flight.

3.3. Comparison With TRMM Microwave Imager (TMI) Observations

[15] This section describes a comparison between satellite measurements from TMI and simulations from four coincident ECMWF analyses in 2000.

3.3.1. Observation and Model Data

[16] Four global meteorological fields have been extracted from the ECMWF archive (one for each season

Table 6. Comparison Between Measurements and Simulations Using GUILLOU_ELLISON[a]

Channel	Bias, K	Standard Deviation, K	Correlation Coefficient	Regression Coefficient	
				Slope	Intercept
10 V	0.44	4.00	0.62	0.92	14.06
10 H	2.01	6.50	0.27	0.99	3.79
19 V	1.49	3.98	0.94	0.99	4.32
19 H	3.49	7.26	0.92	1.00	4.24
21 V	2.83	5.33	0.96	0.97	8.62
37 V	5.77	6.62	0.91	1.10	−16.11
37 H	5.39	8.19	0.87	1.13	−13.95
85 V	5.59	6.36	0.96	0.98	11.39
85 H	7.35	10.49	0.94	10.6	−7.08

[a]Instrument used is TMI 5431 pts.

Table 7. Comparison Between Measurements and Simulations Using GUILLOU_NEW[a]

Channel	Bias, K	Standard Deviation, K	Correlation Coefficient	Regression Coefficient	
				Slope	Intercept
10 V	0.42	4.00	0.62	0.92	14.01
10 H	1.99	6.50	0.27	0.99	3.77
19 V	1.47	3.97	0.94	0.99	4.26
19 H	3.48	7.25	0.92	1.00	4.22
21 V	2.82	5.33	0.96	0.97	8.57
37 V	3.77	4.95	0.91	1.06	−9.78
37 H	3.97	7.31	0.87	1.11	−12.39
85 V	4.03	5.11	0.96	1.02	−0.09
85 H	5.97	9.73	0.94	1.08	−13.11

[a]Instrument used is TMI 5431 pts.

of 2000), containing analyses of surface parameters (temperature, pressure, and wind) and profiles of atmospheric parameters (temperature, water vapor, and cloud liquid water content). The 60 levels in the model allow a complete description of the troposphere/stratosphere profiles, and the horizontal resolution is 0.5°. Locations for which cloud liquid water content is higher than 100 g m^{-2} are excluded on the basis of the TMI liquid water retrieval algorithm. For each field, satellite measurements are selected which are within ±30 min of the analysis time. Observations are averaged to the model resolution.

3.3.2. Comparison of GUILLOU_ELLISON With GUILLOU_NEW Using TMI Observations and European Centre for Medium-Range Weather Forecasts (ECMWF) Meteorological Data

[17] Table 6 contains the results of the comparison using GUILLOU_ELLISON. Comparisons are characterized by the number of points, by the bias (simulations-measurements), by the standard deviation, by the correlation coefficient, and finally by the coefficients of the regression line. Table 7 is the same comparison using the GUILLOU_NEW model. In these comparisons the model of *Liebe et al.* [1993] is used for the atmospheric opacity.

[18] Agreement between measurements and simulations is satisfactory, except for the 10.7 GHz channel where the correlation coefficient is very low. This could be due to the associated spatial resolution (contamination by clouds/rain) or the inadequacies of the surface emissivity model at this frequency (e.g., the effect of wind direction, the inaccuracy in the foam model, and the unsuitability of the geometric optics model). The GUILLOU_NEW model gives a better

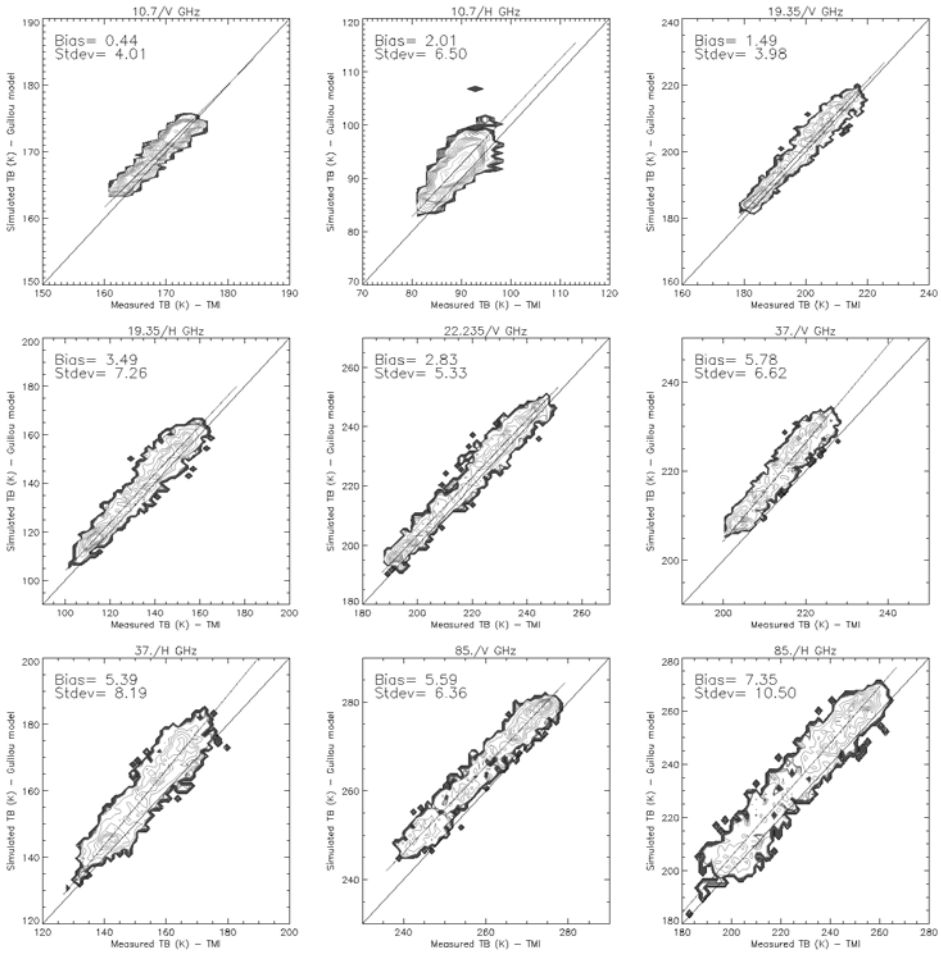

Figure 5. Comparison of measurements and simulations for the *Guillou et al.* [1998] model. See color version of this figure in the HTML.

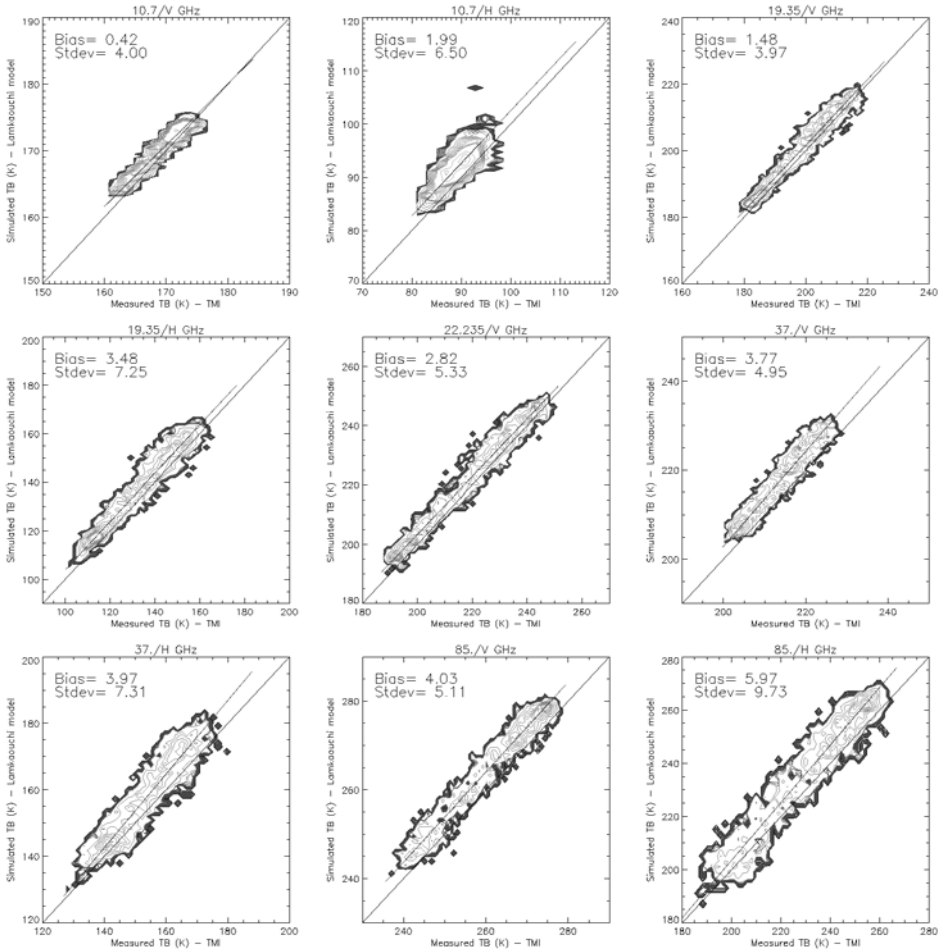

Figure 6. Comparison of TRMM Microwave Imager observations and simulations using the new model. See color version of this figure in the HTML.

fit to the TMI observations above 30 GHz. As this is a clean comparison of the permittivity models this improvement must arise from the new permittivity model. This comparison concludes that the SST dependence of permittivity achieved using the new permittivity model agrees more closely with TMI observations than using the work of *Guillou et al.* [1998]. Figures 5 and 6 show the scatterplots obtained between measurements and simulations for the nine TMI channels and the two different emissivity models.

3.4. Comparison of RTTOV_NEW With RTSSMI_KS Using Special Sensor Microwave Imager Observations and ECMWF Meteorological Data

[19] Total column water vapor and near-surface (10 m) wind speed derived from SSM/I radiances have been operationally assimilated at ECMWF since 1997 and 1999, respectively. The methodology is based on the one-dimensional variational retrieval (1-D-Var) framework [*Phalippou*, 1996] which uses RTSSMI_KS. Model biases (including systematic radiative transfer modeling and instrument calibration errors) are corrected as described by *Harris and Kelly* [2001]. There is a small difference in the radiative transfer model used between RTSSMI_KS and RTTOV_NEW; RTSSMI_KS uses *Liebe* [1989], whereas RTTOV_NEW uses *Liebe* [1989] for water vapor and *Liebe et al.* [1992] for oxygen. This difference is not important for the data shown.

[20] Figures 7 and 8 summarize the 5 day (6–10 May 2001) observation minus first-guess statistics for all seven SSM/I channels of DMSP F-14 from RTSSMI_KS and RTTOV_NEW, respectively. A thorough examination of the difference between RTSSMI_KS and RTTOV_NEW [*Deblonde*, 2000] concluded that at low wind speed the dielectric model was most important, whereas at high wind speed choice of foam model and treatment of multiple reflections can be equally important. The comparisons shown here are for global data, covering a wide range of wind speeds, so reflect the total effect of all the differences between RTSSMI_KS and RTTOV_NEW, not just the dielectic model. Figures 9 and 10 show similar results for NOAA-16 AMSU-A channels 1–6 and 15. Tables 9 and 10 compile the means and standard deviations of the departures. Shown are uncorrected (FG^u) and bias-corrected (FG^c) first-guess departures as well as analysis departures (AN). Note that the data was screened for cloud contamination using simple regression-type algorithms for SSM/I [*Karstens et al.*, 1994] and AMSU-A [*Weng et al.*, 2000] and a cloud liquid-water threshold of 10 g m^{-2} which is lower than the cloud threshold in section 3.4.

[21] Comparing Figures 7 and 8, it becomes evident that RTTOV_NEW gives a closer fit to SSM/I observations than

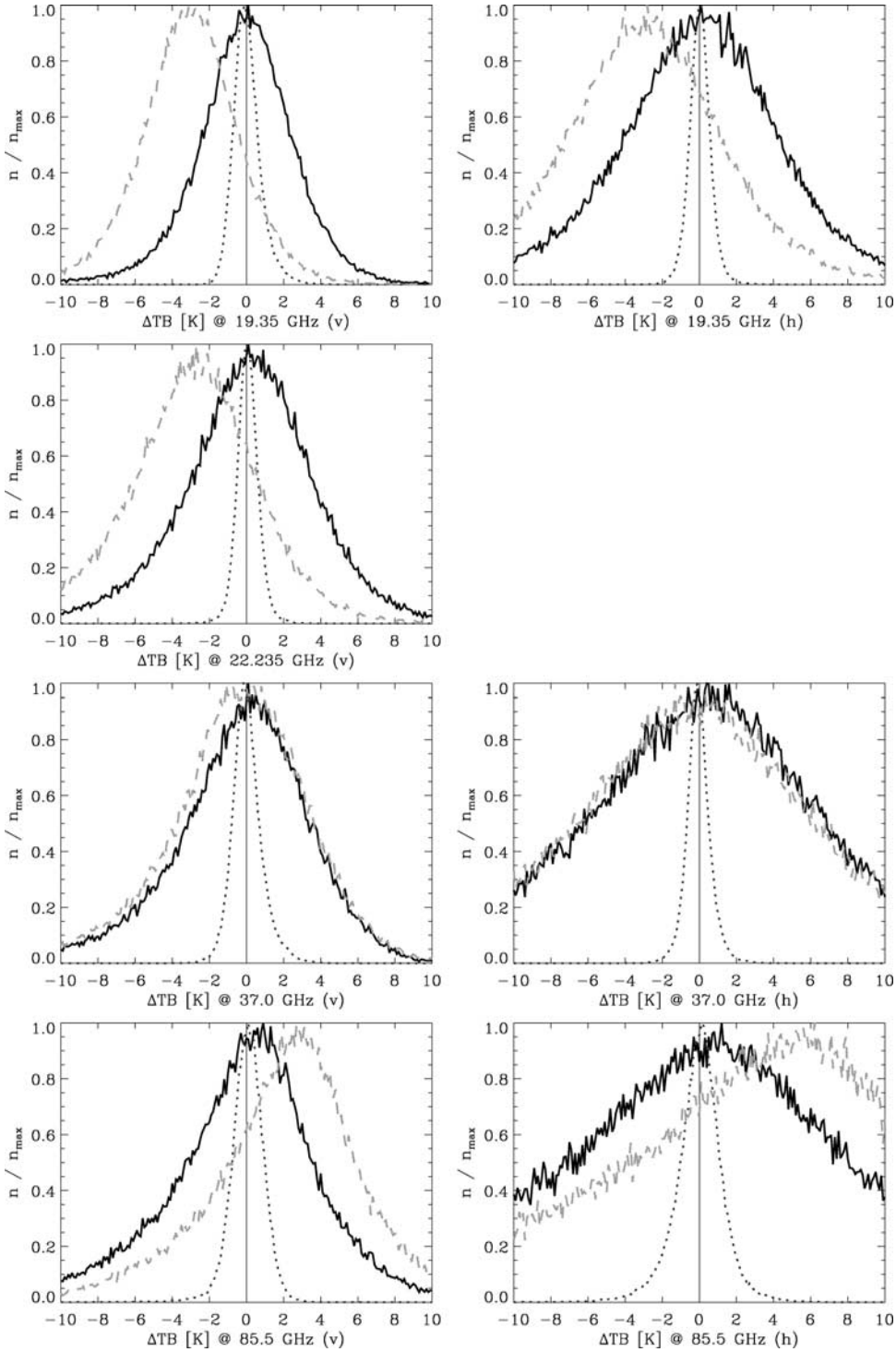

Figure 7. Uncorrected (FG^u; dashed line), bias-corrected (FG^c; solid line), and analysis departures (AN; dotted line) (observation minus model first-guess) from DMSP F-14 Special Sensor Microwave Imager data using RTSSMI for period 06–10/05/2001. See color version of this figure in the HTML.

RTSSMI_KS in terms of both average departures and average spread of the distributions. At 19.35 GHz, almost no bias is observed which is explained by the improved seawater permittivity model. Despite the explicit treatment of geometric optics in RTSSMI_KS, the sensitivity to surface roughness seems to be reproduced as accurately as in RTTOV_NEW where this effect is only parameterized. Another obvious effect is the difference in width for the horizontally polarized channels that respond rather sensitively to surface roughness and atmospheric optical depth. On average, RTTOV produces half the spread in the histogram that are generated by RTSSMI_KS (see

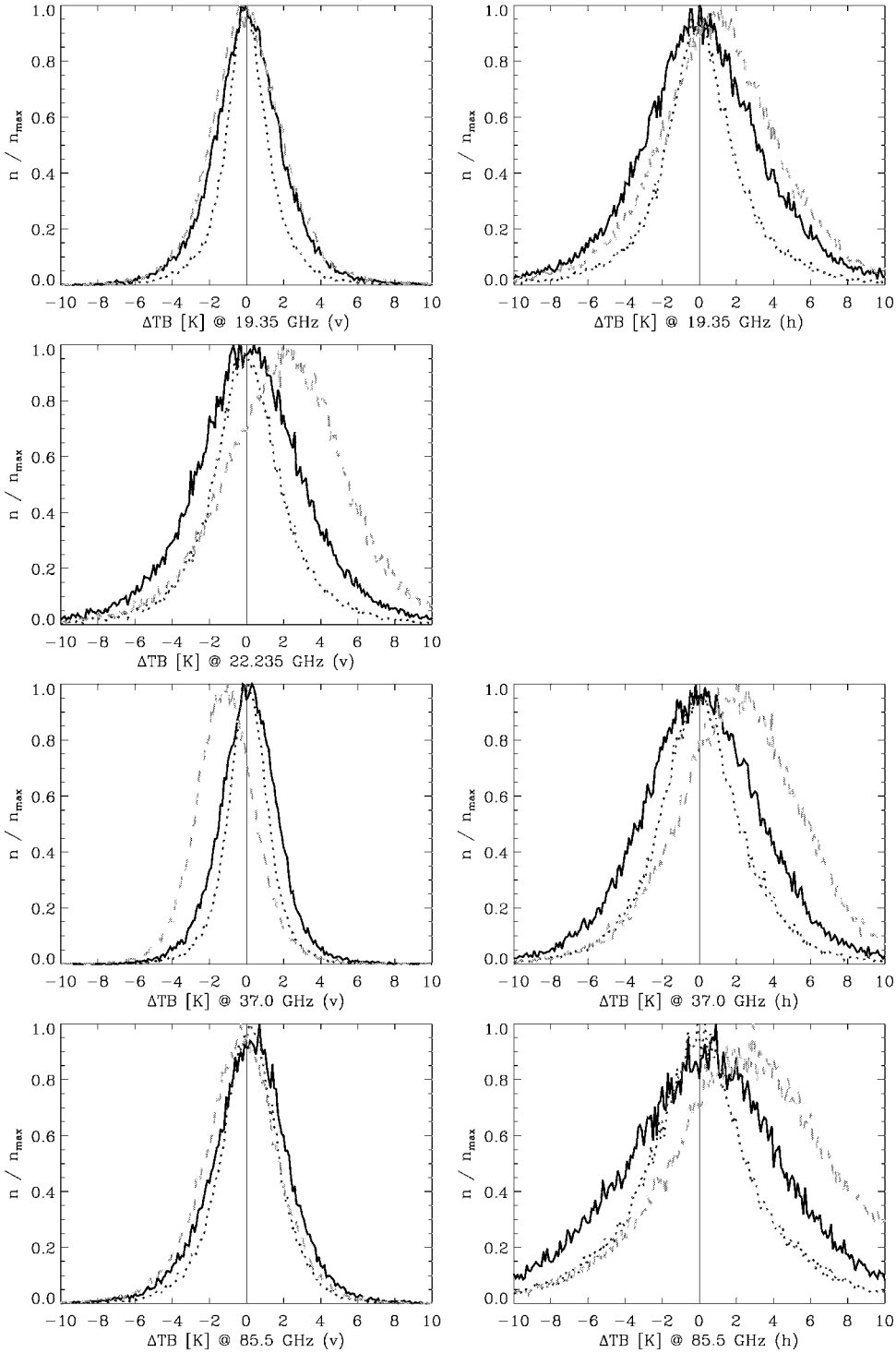

Figure 8. Same as Figure 7 for RTTOV. See color version of this figure in the HTML.

Table 8), which is a consequence of the modification of effective incidence angle for downwelling radiances as a function of opacity and the different model for foam.

3.5. Comparison RTTOV_NEW With RTTOV_ULABY Using Advanced Microwave Sounding Unit Observations and ECMWF Meteorological Data

[22] AMSU-A radiances have been directly assimilated at ECMWF using RTTOV_ULABY. For the comparisons shown, the ECMWF model resolution was reduced from T_L511 to T_L159 (for both inner and outer minimisation loop) and to the 3-D-Var assimilation configuration to allow a more efficient performance. Since the evaluation only aimed at model first-guess versus observation comparisons, this reduction in model performance was considered acceptable. The view geometry for AMSU is different to the SSM/I and TMI considered in previous sections. It has a variable view angle resulting from the cross-track scanning mechanism. As shown by *Deblonde* [2000], the sensitivity to different

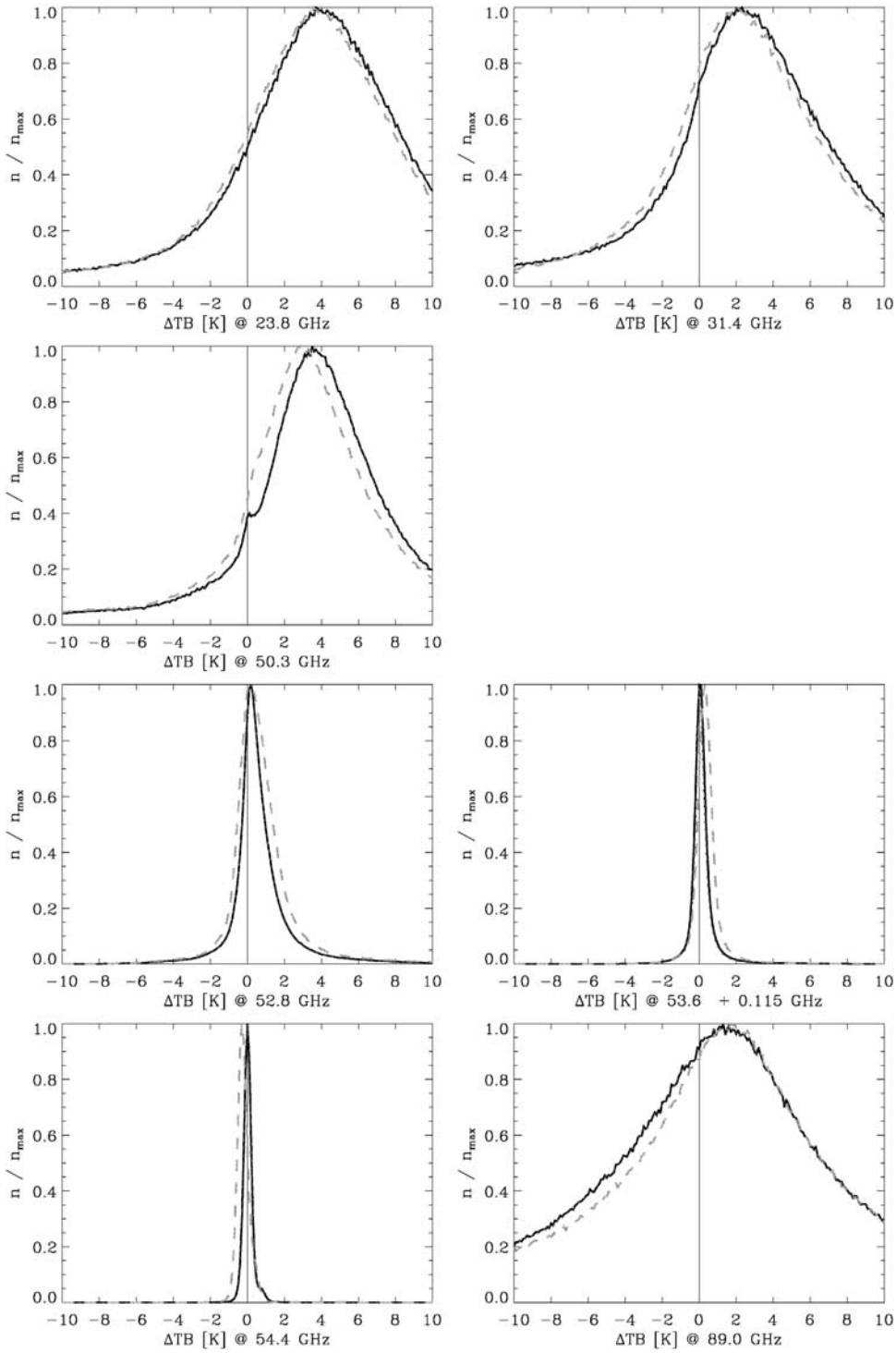

Figure 9. Same as Figure 7 for NOAA-16 Advanced Microwave Sounding Unit-A channels 1–6 and 15. See color version of this figure in the HTML.

aspects of the surface emission model depends on view geometry, and approaches optimized for the SSM/I may not work well for AMSU and vice versa. Both RTTOV_ULABY and RTTOV_NEW use the same atmopspheric model [*Rosenkranz*, 1998].

[23] The differences for AMSU-A channels 1–6 and 15 (Figures 9 and 10) are less obvious but still noticeable. Biases remaining after bias correction are generated by including all data in the statistics while the bias correction is only tuned to a reduced set of data which is actively used in the assimilation system (Table 9). Again, the RTTOV_NEW distributions are slightly less biased while the standard deviations are similar. Once surface contributions to the total signal are small, the statistics are very similar. A remaining issue is the non-Gaussian shape of the lower frequency window channel histograms (Figures 9 and 10), in particular at 31.4 GHz. The shape of the distribution in Figure 7 may suggest that this is the

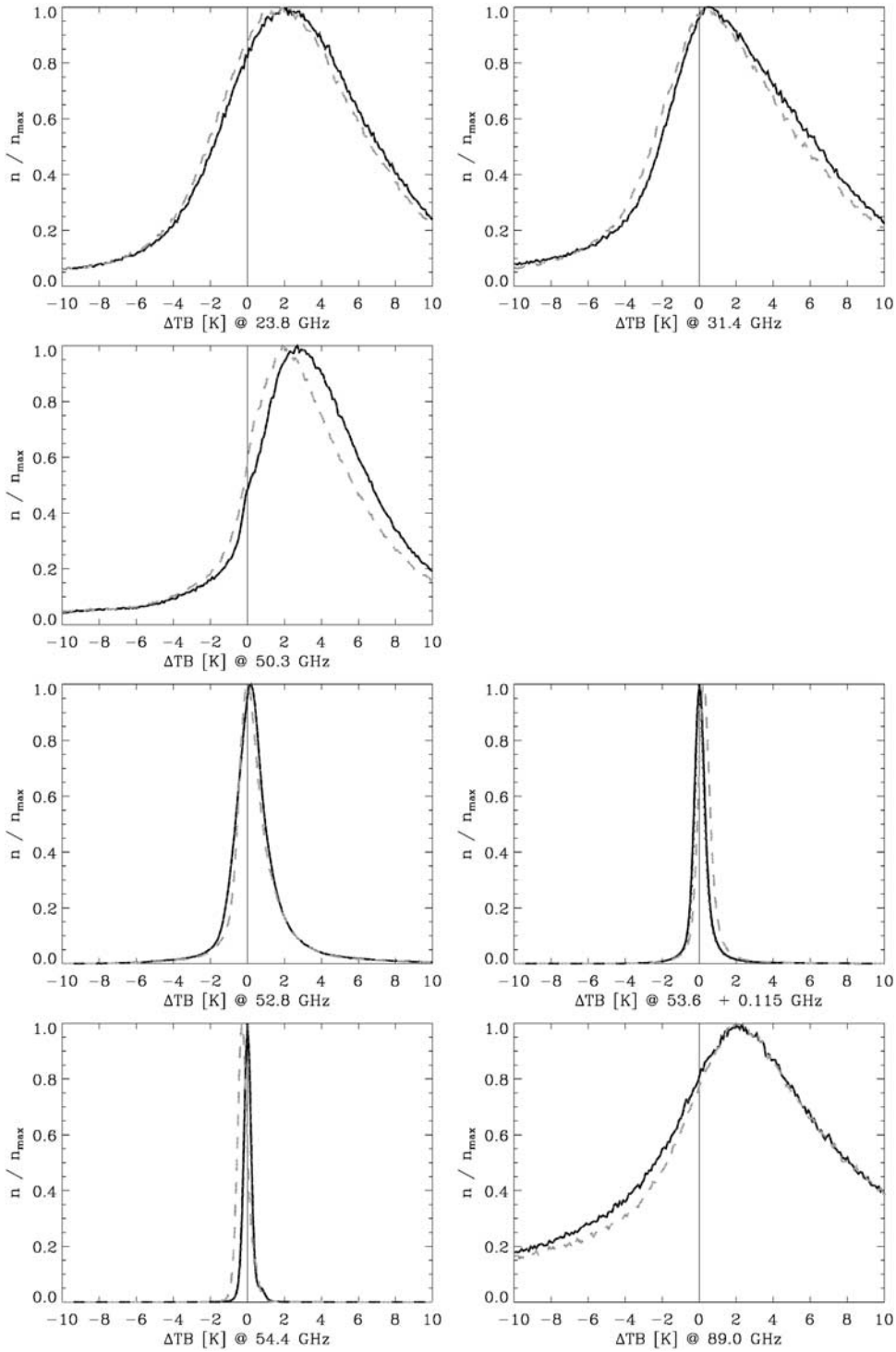

Figure 10. Same as Figure 8 for RTTOV. See color version of this figure in the HTML.

influence of the horizontally polarized component of the emissivity even though it is only weakly expressed in the SSM/I statistics.

[24] The lack of any significant advantage of the RTTOV_NEW model over RTTOV_ULABY may be considered to be a surprising result given the new science available to RTTOV_NEW. A similar study at the Met Office found no significant benefit in using the RTTOV_NEW formulation over a model using the work of *Guillou et al.* [1998]. However, one using the permittivity model of *Klein and Swift* [1977] did give substantial biases. Therefore in contrast to the TMI results in section 3.3 no obvious advantage is found for the double Debye form for modeling AMSU over the best performing single Debye models.

3.6. Comparison of RTSSMI_KS and RTTOV_NEW With Observations From Airborne Radiometers and In Situ Meteorological Data

[25] The results in section 2 show the largest differences for cold sea surface temperatures. During the Measurement

Table 8. Means and Standard Deviations of Uncorrected, Bias-Corrected First-Guess and Analysis Departures From Defense Meteorites Satellite Program F-14 SSM/I Data Using RTSSMI_KS and RTTOV_NEW Models for the Period 6–10 May 2001[a]

	Average			Standard deviation		
Channel	*FGu*	*FGc*	Analysis	*FGu*	*FGc*	Analysis
			RTSSMI_KS			
19.35 V	−3.2	−0.2	0.0	3.0	3.0	0.8
19.35 H	−3.4	−0.3	0.0	5.4	5.5	0.6
22.235 V	−3.1	−0.0	0.1	4.0	4.0	0.6
37 V	−0.8	−0.7	0.0	4.6	4.5	0.8
37 H	−1.7	−1.3	0.0	9.1	9.0	0.7
85.5 V	1.9	−0.4	0.0	4.5	4.5	1.1
85.5 H	2.1	−1.0	0.0	11.4	10.	1.4
			RTTOV_NEW			
19.35 V	0.1	0.1	0.1	2.2	2.1	1.7
19.35 H	1.1	0.2	0.1	3.9	3.8	3.0
22.235 V	2.0	0.1	0.0	3.7	3.5	2.7
37 V	−1.1	0.1	0.1	1.8	1.7	1.4
37 H	2.2	0.2	0.1	3.6	3.6	2.9
85.5 V	−0.4	0.1	0.1	2.3	2.3	2.0
85.5 H	3.0	0.1	−0.1	5.5	5.3	4.3

[a]Units are in kelvin, sample size ~50,000. FG^u, uncorrected; FG^c, bias-corrected first guess. Departures are given as observation minus model first-guess.

of Tropospheric Humidity (MOTH) Arctic experiment (December 1999), several aircraft flights were performed in cold dry weather conditions over the Baltic Sea (59°N, 20°E). The measurements were taken over the open ocean with wind speeds reaching up to 18 m s^{-1}. The atmospheric absorption models in RTSSMI_KS and RTTOV_NEW is discussed in section 3.4.

3.6.1. Description of Aircraft Runs and Meteorological Observations

[26] Aircraft runs were performed in cold dry atmospheres over the open ocean. Table 10 describes the different runs and some of the ancillary observations. There were a total of 12 runs with 10 m wind speeds ranging between 9.9 and 18.2 m s^{-1} and total column water vapor ranging from 4.2 to 9.3 kg m^{-2}. Skin temperature measurements were retrieved from a Heimann infrared radiometer (8–15 μm), which has a quoted accuracy of ±0.5°C. Profiles of temperature and humidity were measured by the aircraft from 15 m to 7–8 km. The wind speed near the surface was also obtained from dropsonde measurements at a nominal 10 m height, with a quoted accuracy of ±0.5 m s^{-1}. However, as these sondes drop at 12 m s^{-1}, and only report twice a second, the actual altitude could be in error by up to 6 m.

[27] In Table 10, aircraft runs with the same flight number (e.g., flight A740 has four runs) used the same meteorological fields in the radiative transfer calculations except for the skin temperature and the static pressure at aircraft level (both are listed in Table 10). Profiles of meteorological observations were constructed by extracting data at a reduced number of vertical levels. The resulting number of levels for the radiosonde/dropsonde profiles used varied between 95 and 98 levels depending on the flight. Deimos viewed downward in five positions between nadir and 40° forward. MARSS viewed downward in nine positions, ranging from 46.1° forward of nadir to 36.4° backward of nadir. MARSS also measured nine zenith views in the opposite directions.

Table 9. NOAA-16 AMSU-A Data Using the RTTOV_ULABY Model[a]

	Average			Standard deviation		
Channel	*FGu*	*FGc*	Analysis	*FGu*	*FGc*	Analysis
			RTTOV_ULABY			
23.8	5.7	6.0	6.0	12.5	12.5	12.5
31.4	4.9	5.2	5.2	13.3	13.3	13.3
50.3	4.5	5.1	5.1	7.4	7.3	7.3
52.8	0.9	0.9	0.9	2.4	2.4	2.4
89	0.6	0.2	0.2	11.2	11.3	11.3
			RTTOV_NEW			
23.8	4.2	4.5	4.5	12.0	12.0	12.0
31.4	4.1	4.4	4.4	13.1	13.2	13.2
50.3	4.3	4.9	4.9	7.5	7.5	7.5
52.8	0.8	0.7	0.7	2.4	2.4	2.4
89	2.6	2.1	2.1	12.4	12.5	12.5

[a]Units are in kelvin.

Table 10. Met Office C-130 Flights Used in This Analysis From the MOTH-Arctic Experiment

Aircraft Flight and Runs	Total Column Water Vapor, kg m^{-2}	Surface Air Temperature, °C	10 m Dropsonde Wind Speed, ms^{-1}
A739 R2.1, R3.1	9.3	6.9 ± 0.1	18.2 ± 0.4
A739 R2.2, R3.2	9.3	6.8 ± 0.1	18.2 ± 0.4
A740 R2.1, R3.1	6.1	5.3 ± 0.2	15.0 ± 1.3
A740 R2.2, R3.2	6.1	5.5 ± 0.2	15.0 ± 1.3
A740 R2.3, R3.2	6.1	5.3 ± 0.1	15.0 ± 1.3
A740 R2.4, R3.4	6.1	5.2 ± 0.2	15.0 ± 1.3
A742 R2.1, R3.1	4.2	3.8 ± 0.1	9.9 ± 1.5
A742 R2.2, R3.2	4.2	3.6 ± 0.1	9.9 ± 1.5
A742 R2.3, R3.2	4.2	4.3 ± 0.4	9.9 ± 1.5
A742 R2.4, R3.4	4.2	3.7 ± 0.3	9.9 ± 1.5
A744 R3.1, R4.1	8.8	5.2 ± 0.1	12.4 ± 1.0
A744 R3.2, R4.2	8.8	5.1 ± 0.2	12.4 ± 1.0

3.6.2. Aircraft Validation

[28] Statistics for different combinations of models (RTSSMI or RTTOV) are listed in Tables 11 and 12. These use the same atmospheric model [*Rosenkranz*, 1998] to allow for the atmosphere between the aircraft and the surface. The sensitivity to this choice of atmospheric model was tested by repeating using the other models [*Liebe*, 1989; *Liebe et al.*, 1993]. At 23.8 GHz, this made little difference, but at higher frequencies the calculated brightness temperatures using the work of *Rosenkranz* [1998] are between 0.3 and 1.2 K lower than using *Liebe* [1989]. The standard deviations have been computed after removal of scan-position-dependent biases, covering the full range of view angles used by AMSU and SSM/I. Note that the Bragg term by *English and Hewison* [1998] gives a large improve-

Table 11. RTSSMI and RTM Models Versus Deimos Measurements[a]

Model	Bias (Obs.-Model), K	Standard Deviation, K
	Frequency 23.8 GHz	
RTSSMI_KS	4.95	2.75
RTTOV_NEW	1.62 (4.40)	2.60 (3.03)
	Frequency 50.1 GHz	
RTSSMI_KS	1.11	2.37
RTTOV_NEW	2.53 (2.91)	3.18 (3.28)

[a]Note that for the Deimos channels, the results at the 40° view angle were excluded due to aircraft fuselage contamination in the forward view. Results with the Bragg term in the work of *English and Hewison* [1998] switched off are given in parentheses.

Table 12. RTSSMI_KS and RTTOV_NEW Model Versus MARSS Measurements

Model	Bias (Obs.-Model), K	Standard Deviation, K
	Frequency 89 GHz	
RTSSMI_KS	−6.00	3.36
RTTOV_NEW	−0.95 (−0.84)	2.37 (2.36)
	Frequency 157 GHz	
RTSSMI_KS	−5.04	1.68
RTTOV_NEW	−0.13 (−0.15)	1.99 (1.99)
	Frequency 183±7 GHz	
RTSSMI_KS	−0.92	0.99
RTTOV_NEW	0.74 (0.74)	1.02 (1.02)

ment in the bias at 23.8 GHz. The comparison with this term switched off is also given, so that the impact of the permittivity model alone can be identified. At other frequencies the Bragg term makes little difference to the calculated brightness temperatures.

[29] At 23.8 GHz, RTSSMI_KS gives lower mean brightness temperatures than the new model, arising from the absence of a Bragg term, whereas at 50.1, 89, 150, and 183 GHz, RTTOV_NEW gives lower mean brightness temperatures. This results in a lower mean error using the new data for all channels except 50.1 GHz. For the 50.1 GHz channel, the RTSSMI_KS provides the lowest bias and standard deviation.

4. Conclusions

[30] A new model for permittivity of seawater at frequencies up to 100 GHz has been presented. It has been compared to several different sources of observations by groups in four different centers using three different sources of meteorological data (two independent NWP models compared to AMSU data, SSM/I data, TMI data, and in situ data compared to aircraft radiometer data) involving implementation within three different radiative transfer models. This scope of testing allows for both clean comparisons of the permittivity models themselves, but also a comparison of other components of the emissivity models. The clean comparison of the permittivity model (section 3.3) showed an improvement in the fit to TMI observations using either the new model compared to using the work of *Ellison et al.* [1998]. The comparisons in sections 3.4 and 3.5 are not clean, as more than just the permittivity model has been changed. The improvement in fit for SSM/I is larger than would be expected from the permittivity change alone. It is likely therefore that improvement also arises either from the different foam model, or the way in which reflected downwelling radiance is handled. By contrast, the results in section 3.5 for AMSU show the expected improvement in bias but actually show a degradation in terms of standard deviation. This leads to the conclusion that the empirical treatment of roughness [*Ulaby et al.*, 1986] gives a particularly good fit to AMSU. Finally the aircraft validation, which focused on cold seas where the largest permittivity model differences occur, showed mixed results. At 23.8, 89, and 150 GHz the results were as expected with a substantial improvement in bias. However, at 50.1 GHz the bias was worse using the new model. This may suggest that other sources of bias for this channel are important. These results were all obtained at high wind speed, so the treatment of roughness and foam will tend to be at least as important, if not more important, than the permittivity model [*Deblonde*, 2000].

[31] There are some robust conclusions which are common to all the experiments, and by other comparisons not all of which could be included. The *Klein and Swift* [1977] model gives a bias which is very significantly improved using the work of either *Guillou et al.* [1998] or the new permittivity model. There is reasonable evidence that the new model is giving better results than *Guillou et al.* [1998] for TMI at high frequency, although this result is not repeated in comparison against AMSU.

Appendix A

[32] The Debye model is

$$\varepsilon(\nu,t) = \varepsilon'(\nu,t) - j\varepsilon''(\nu,t) = \frac{\varepsilon_S - \varepsilon_\infty}{1 + j2\pi\tau\nu} - j\frac{\sigma}{2\pi\varepsilon^*\nu} + \varepsilon_\infty,$$

where $\varepsilon^* = 8.854 \times 10^{-12}$ and σ, the conductivity of seawater with a salinity of 35‰ as a function of temperature T in degrees Celsius, is given by $\sigma = 2.906 + 0.094374T$. The calculated values of the parameters from data in the range 3–20 GHz are given below. Tables 1 and 2 present the new permittivity data for seawater over the frequency range 30–105 GHz and over the temperature range −2°–30°C.

[33] **Acknowledgments.** W. J. Ellison, A. Balana, and K. Lamkaouchi would like to thank E.S.A. for financial support, and in particular we thank J. Noll and M. Winter (E.S.A./ESTEC) for all their help during the course of the measurement campaign.

References

Barthel, J., K. Buchhuber, R. Buchner, and H. Hetzenauer, Dielectric spectra of some common solvents: Water and lower alcohols, *Chem. Phys. Lett.*, *165*, 369–373, 1990.

Barthel, J., K. Bachhuber, R. Buchner, H. Hetzenauer, and M. Kleebauer, A computer controlled system of transmission lines, *Ber. Bunsenges. Phys. Chem.*, *95*(8), 583–588, 1991.

Barthel, J., H. Hetzenauer, and R. Buchner, Dielectric relaxation of aqueous electrolytic solutions, *Ber. Bunsenges. Phys. Chem.*, *96*(8), 988–997, 1992.

Deblonde, G., Evaluation of fastem and fastem2, Met Off., Exeter, UK, 2000.

Deblonde, G., and S. J. English, Evaluation of the fastem2 fast microwave oceanic surface emissivity model, paper presented at Technical Proceedings of the 11th International ATOVS Study Conference, Int. Radiat. Comm., Budapest, Hungary, 20–26 September 2000.

Ellison, W. J., K. Lamkaouchi, and J. M. Moreau, Water: A dielectric reference, *J. Mol. Liq.*, *68*, 171–279, 1996.

Ellison, W. J., A. Balana, and K. Lamkaouchi, Dielectric properties of sea water in the range 30–105 GHz: Final report, *ESTEC/ESA Contract 11197/97/NL/CN*, Eur. Space Agency, Paris, 1997.

Ellison, W. J., A. Balana, G. Delbos, K. Lamkaouchi, L. Eymard, C. Guillou, and C. Prigent, New permittivity measurements of seawater, *Radio Sci.*, *33*(3), 639–648, 1998.

English, S. J., Estimation of temperature and humidity profile information from microwave radiances over different surface types, *J. Appl. Meteorol.*, *38*, 1526–1541, 1999.

English, S. J., and T. J. Hewison, A fast generic millimeter-wave emissivity model, *Proc. SPIE*, *3503*, 288–300, 1998.

English, S. J., R. J. Renshaw, P. C. Dibben, A. J. Smith, P. J. Rayer, C. Poulsen, F. W. Saunders, and J. R. Eyre, A comparison of the impact of TOVS and ATOVS satellite sounding data on the accuracy of numerical weather forecasts, *Q. J. R. Meteorol. Soc.*, *136*, 2911–2931, 2000.

Eyre, J. R., A fast radiative transfer model for satellite sounding systems, *ECMWF Tech. Memo. 176*, European Centre for Medium-Range Weather Forecasts, Reading, UK, 1991.

Grant, E. H., and R. J. Sheppard, Dielectric relaxation in water in the neighborhood of 4°C, *J. Chem. Phys.*, *60*(5), 1792–1796, 1974.

Grassholf, K., *Methods of Sea Water Analysis*, 317 pp., Verlag-Chemie, New York, 1976.

Guillou, C., W. J. Ellison, L. Eymard, K. Lamkaouchi, C. Prigent, G. Delbos, A. Balana, and S. A. Boukabara, Impact of new permittivity measurements on sea-surface emissivity modelling in microwaves, *Radio Sci.*, *33*(3), 649–667, 1998.

Haggis, G. H., J. B. Hasted, and T. J. Buchanan, The dielectric properties of water in solutions, *J. Chem. Phys.*, *20*(20), 1452–1464, 1952.

Harris, B. A., and G. Kelly, A satellite radiance-bias correction scheme for data assimilation, *Q. J. R. Meteorol. Soc.*, *127*, 1453–1468, 2001.

Hewison, T. J., The design of Deimos: A microwave radiometer with channels at 23.8 GHz and 50.3 GHz for the UK Meteorol. Research Flight C-130 aircraft, in *Proc. Int. Geosci. and Remote Sens. Symp.*, pp. 2261–2263, IEEE Geosci. Remote Sens. Soc., Florence, Italy, 1995.

Karstens, U., C. Simmer, and E. Ruprecht, Remote sensing of cloud liquid water, *Meteorol. Atmos. Phys.*, *54*, 157–171, 1994.

Klein, L. A., and C. T. Swift, An improved model for the dielectric constant of sea water at microwave frequencies, *IEEE Trans. Antennas and Propag.*, *25*, 104–111, 1977.

Lamkaouchi, K., A. Balana, G. Delbos, and W. J. Ellison, Permittivity measurements of lossy liquids in the frequency range 20–110 GHz, *Meas. Sci. Technol.*, *14*, 1–7, 2003.

Liebe, H. J., MPM—An atmospheric millimeter wave propogation model, *Int. J. Infrared Millimeter Waves*, *10*, 631–650, 1989.

Liebe, H. J., G. A. Hufford, and T. Manabe, A model for the permittivity of water at frequencies below 1 THz, *Int. J. Infrared Millimeter Waves*, *12*, 659–675, 1991.

Liebe, H. J., P. W. Rosenkranz, and G. A. Hufford, Atmospheric 60 GHz oxygen spectrum: New laboratory measurements and line parameters, *J. Quant. Spectrosc. Radiat. Transfer*, *48*, 629–643, 1992.

Liebe, H., G. Hufford, and M. Cotton, Propagation modeling of moist air and suspended water/ice particles at freuquencies below 1000 GHz, paper presented at AGARD 52 Specialist Meeting of the Electromagnetic Wave Propagation Panel, Palma de Mallorca, Spain, 17–21 May 1993.

McGrath, A., and T. J. Hewison, Measuring the accuracy of a microwave airborne radiometer (MARSS)—An airborne microwave radiometer, *J. Atmos. Oceanic Technol.*, *18*(12), 2003–2012, 2001.

Phalippou, L., A microwave radiative transfer model, *ECMWF Tech. Memo 190*, 12 pp., Eur. Cent. for Med. Range Weather Forecasts, Reading, UK, 1993.

Phalippou, L., Variational retrieval of humidity profile, wind speed and cloud liquid-water path with SSM/I: Potential for numerical weather prediction, *Q. J. R. Meteorol. Soc.*, *122*, 327–355, 1996.

Rosenkranz, P. W., Water vapor microwave continuum absorption: A comparison of measurements and models, *Radio Sci.*, *33*(4), 919–928, 1998.

Saunders, R. W., P. Brunel, F. Chevallier, G. Deblonde, S. J. English, M. Matricardi, and P. J. Rayer, *RTTOV-7 Science and Validation Rep., NWP Div. Tech. Memo. 387*, Met Off., Bracknell UK, 2002.

Stogryn, A. P., H. T. Bull, K. Ruayi, and S. Iravanchy, The microwave permittivity of sea and fresh water, *Aerojet Internal Report*, Aerojet, Sacramento, Calif., 1995.

Ulaby, F. T., R. K. Moore, and A. K. Fung, *Microwave Remote Sensing: Active and Passive*, vol. 3, pp. 1065–2137, Artech House, Norwood, Mass., 1986.

Weng, F., T. Zhu, and D. Zhang, Applications of advanced microwave sounding unit to improving the analysis wind field in tropical cyclones, paper presented at 4th Symp. on Integrated Obs. Syst., Am. Meteorol. Soc., Long Beach, Calif., 2000.

A. Balana, Centre d'études nucléaires de Bordeaux Gradignan, F-33174 Gradignan, France.

P. Bauer and G. Kelly, European Centre for Medium-Range Weather Forecasts, Shinfield Park, Reading RG9 6AX, UK.

G. Deblonde, Meteorological Service of Canada, Dorval, Quebec, Canada.

W. J. Ellison, Physique des Interactions Ondes Matières, Ecole Nationale Supérieure de Chimie et de Physique de Bordeaux, 16 avenue Pey Berland, F-33405 Pessac, France.

S. J. English and T. J. Hewison, Met Office, Exeter EX1 3PB, UK. (stephen.english@metoffice.com)

L. Eymard, Centre d'étude des Environnements Terrestre et Planétaires/ Institut Pierre Simon Laplace/Centre National de la Recherche Scientifique, Université St Quentin-Versailles, F-78140 Vélizy, France.

K. Lamkaouchi, Faculty of Sciences, University of Meknès, Morocco, Monaco.

E. Obligis, Space Oceanography Division, Collecte Localisation Satellites, 8-10 rue Hermes, F-31526 Ramonville St-Agne, France.